Electronic Supplementary Material (ESI) for Physical Chemistry Chemical Physics.
This journal is © the Owner Societies 2024

Supplementary information

Enhanced Near-Infrared Optical Transmission in Zinc Germanium Phosphide Crystals via Precise Magnesium Doping

Shichao Cheng [a], Xueyan Zhang [a], Xiangran Kong [a], Tao Liu [a], Jingdong Yan [a], Tetiana Prikhna [b], Yunfei Shang [a,], Zuotao Lei [a,]* and Chunhui Yang [a]*

[a] MIIT Key Laboratory of Critical Materials Technology for New Energy Conversion and Storage, School of Chemistry and Chemical Engineering, Harbin Institute of Technology, Harbin, 150001, People's Republic of China

[b] V. N. Bakul Institute for Superhard Materials of the National Academy of Sciences of Ukraine

Experiment section

X-ray Diffraction. The powder X-ray diffraction patterns were collected by a Bruker D2 PHASER Powder X-ray diffractometer using Cu Kα radiation (λ = 1.54059 Å) at room temperature. The 2θ range was set from 10° to 80°and scan was taken at a step size of 0.01° and a fixed time of 0.5 s. The mercury program was used to calculate simulated patterns from single-crystal reflection data. The X-ray rocking curves of the crystals were measured on PANalytical Empyrean high resolution x-ray diffractometer with Cu Kα radiation (λ = 1.54059 Å).

UV−vis−NIR. UV−Vis−NIR diffuse transmittance was performed at room temperature on a computer-controlled Agilent Carry 5000 UV−vis−NIR spectrometer equipped with an integrating sphere.

Elemental Analysis. The ZGP nanoplate orientated normal to the (001) face with the size of 50 nm was fabricated by focused ion beam-scanning electron microscopy (FIB-SEM) system to be measured by a spherical aberration Cs-STEM (Titan Themis Cubed G2 60-300). The percentage of chemical element content was measured by scanning transmission electron microscopy equipped with energy dispersive X-ray spectroscopy (STEM-EDS). To determine the concentrations of magnesium in the doped samples, glow discharge mass spectrometry (GDMS) measurements were taken using a Nu instruments-Astrum system which provides a ppb/ppt (weight) level detection limit.

Photoluminescence. In addition, PL spectra were collected on a 1 mm-thick ZGP crystal using a spectrometer (TR550MST) with a 532 nm laser. The PL data were obtained from liquid nitrogen using a grating spectrometer and either a PMT (GaAs response), or Ge detector. Temperature-dependent PL spectra of ZGP crystal were collected 100 K. All the luminescence dynamics were recorded with a 500 MHz Tektronix digital oscilloscope.

Electron paramagnetic resonance. The EPR was carried out using a Bruker EMX PLUS spectrometer operating at the X-band (ν ≈ 9.41 GHz). Temperatures in the range

100–300 K were achieved with Oxford Instruments continuous flow cryostats. The sample temperature 100 K for the Zn vacancy signal.

Theoretical Calculation. The Vienna Ab-initio Simulation Package (VASP) was employed to perform all the density functional theory (DFT) calculations. The generalized gradient approximation (GGA) with the Perdew−Buker−Ernzerhof (PBE) functional was adopted[1]. The projected augmented wave (PAW) potentials were chosen to describe the core-electron interactions and take valence electrons into account using a plane-wave basis set with a kinetic energy cutoff of 400 eV. Partial occupancies of the Kohn-Sham orbitals were allowed using the Gaussian smearing method and a width of 0.01 eV. The electronic energy was considered self-consistent when the energy change was smaller than 10^{-6} eV. The Brillouin zone integration was performed using 2×2×1. On the LOBSTER side[2-5], the original basis set and its basic functions (*s*, *p* and *d*) manage to reconstruct the PAW electronic structure. To realize a more accurate description of the bandgap, the Heyd–Scuseria–Ernzerhof (HSE06) hybrid DFT functional was performed.

Defect formation energy of the charge state q dependent on the Fermi level position were calculated in accordance with the literature[6, 7]:

$$\Delta E_f(\alpha, q) = E(\alpha, q) - E(per) - \Delta n_i \mu_i + qE_F$$

where $E(\alpha, q)$ means the total energy calculated from the supercell with defects α in its charge state q, and $E(per)$ is the total energy of the perfect crystal supercells. μ_i is the atomic chemical potential of an atom reservoir of element i, Δn_i is the change in the number of atoms of species i, which has been added ($\Delta n_i > 0$) or removed ($\Delta n_i < 0$). E_F is the Fermi energy referenced to the VBM level.

Table S1. Calculated formation energies of different point defects in ZGP crystals.

	V_{Zn}	V_P	Ge_{Zn}	Ge_P
Defects formation energy	-3.57eV	-4.48 eV	-1.09 eV	2.25eV

Table S2. Calculated total energy of ZGP and ZGP-Mg supercell structures.

	ZGP	ZGP-Mg
Total energy	-548.99 eV	-553.68 eV

Table S3. Calculated cell parameters of ZGP-V_{Zn} and ZGP-Mg structures.

	a (Å)	*b* (Å)	*c* (Å)	*α* (°)	*β* (°)	*γ* (°)
ZGP-V_{Zn}	5.54	5.54	10.09	90	90	90
ZGP-Mg	5.49	5.49	10.74	90	90	90

Table S4. Reported absorption coefficients and optical transmittances at 2 μm of grown ZGP crystals.

Crystal thickness (mm)	Growth Methods	Absorption coefficient for 2.09 μm o light (cm^{-1})	Optical transmittance at 2μm (%)	Reference
1.3	VB[a]	1.3	45	[8]
1.5	VB	-	46	[9]
2.5	VB	0.25	49	[10]
3	VB	-	40	[11]
2	VB	0.12	-	[12]
3	VB	-	49	[13]
10	VB	0.29	-	[14]
2	VB	-	45	[15]
4	VB	-	47	[16]
12	HGF[b]	0.26	-	[17]
6	VB	-	49	[18]
1	VB	0.02	56	This work
6	VB	0.11	50.5	This work

a: vertical Bridgman technique (VB)

b: horizontal-gradient-freeze (HGF)

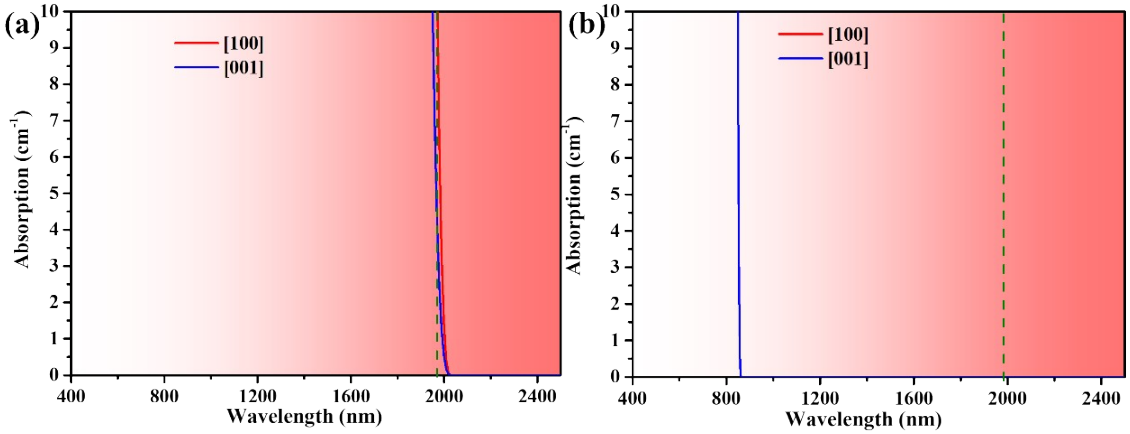

Figure S1. Calculated enlarged optical absorption spectra of the ZGP-V_{Zn} and ZGP-Mg structures.

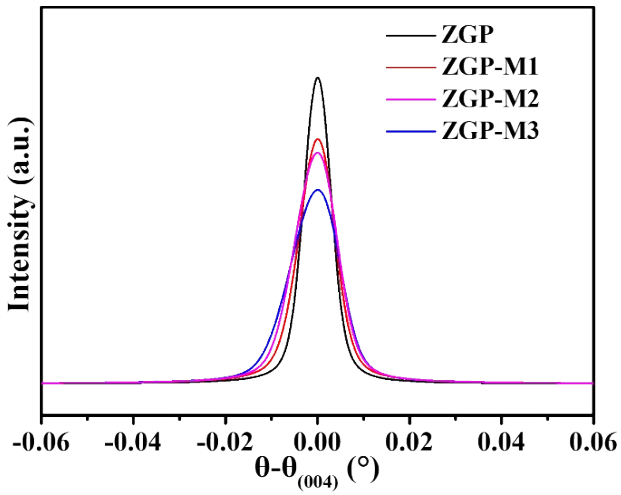

Figure S2. Rocking curves of (004) crystallographic plane in magnesium-doped and undoped ZGP single crystals.

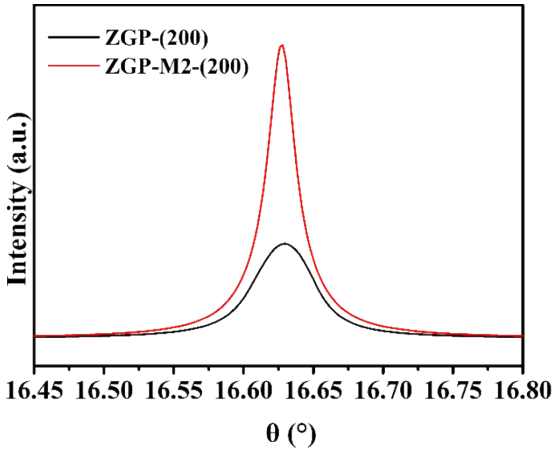

Figure S3. Rocking curves of (200) crystallographic plane in ZGP-M2 and undoped ZGP single crystals.

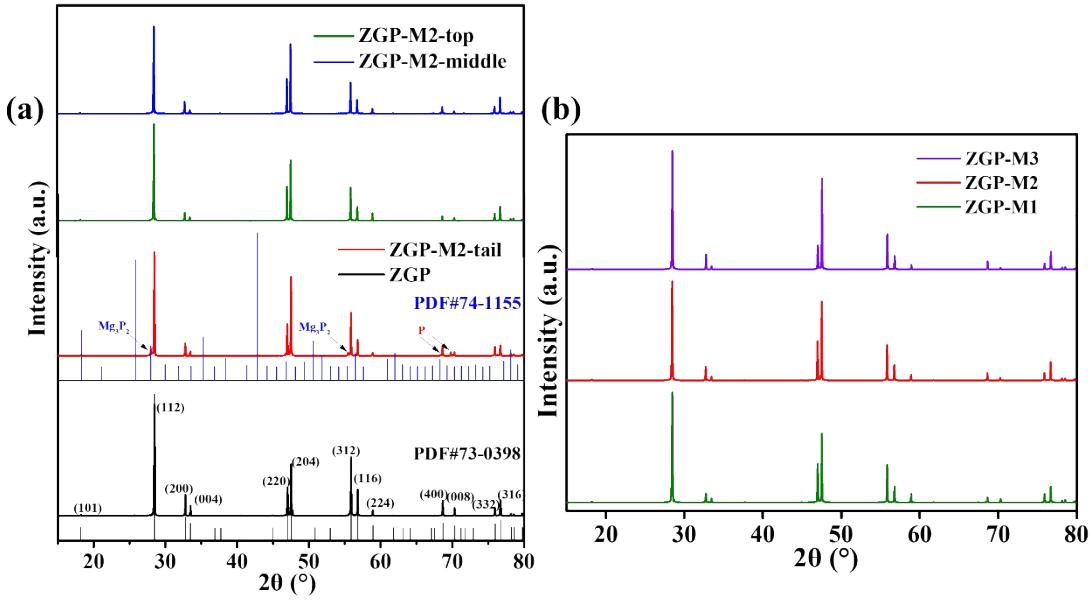

Figure S4. (a) XRD patterns were obtained from different segments of the ZGP-M2 crystals; (b) The XRD patterns specifically from the middle portions of the ZGP-M1, ZGP-M2, and ZGP-M3 crystals.

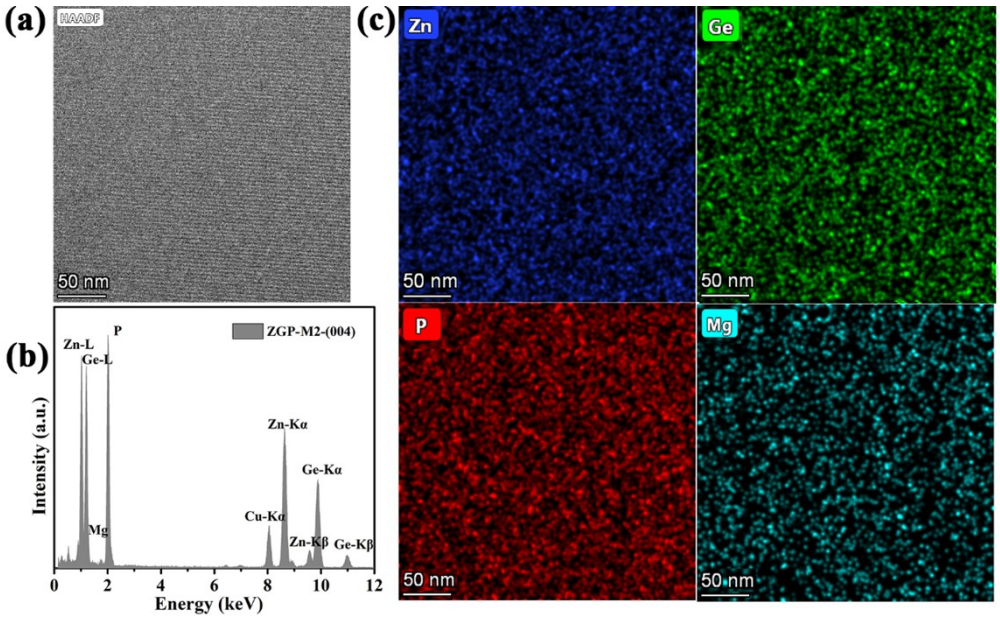

Figure S5. (a) STEM image, (b) STEM-EDS pattern of a ZGP nanoplate and (c) corresponding STEM-EDS chemical element maps.

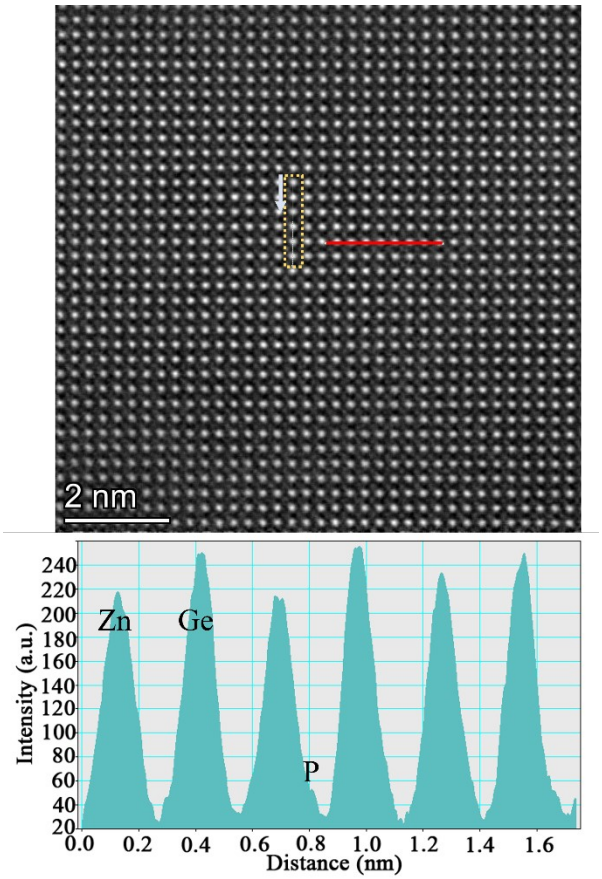

Figure S6. HAADF-STEM images of a chalcopyrite ZGP-M2 nanoplate and intensity profiles recorded by scanning along the direction of the ZGP-M2 (001) plane from the image (yellow line).

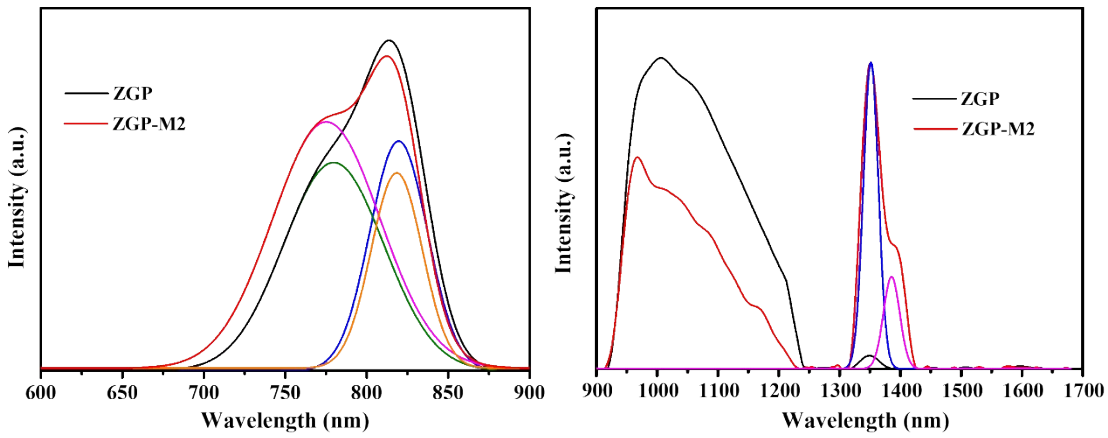

Figure S7. (a) The PL spectra of the samples were recorded at a temperature of 100 K, covering a wavelength range of 600-900 nm and (b) 900-1700 nm.

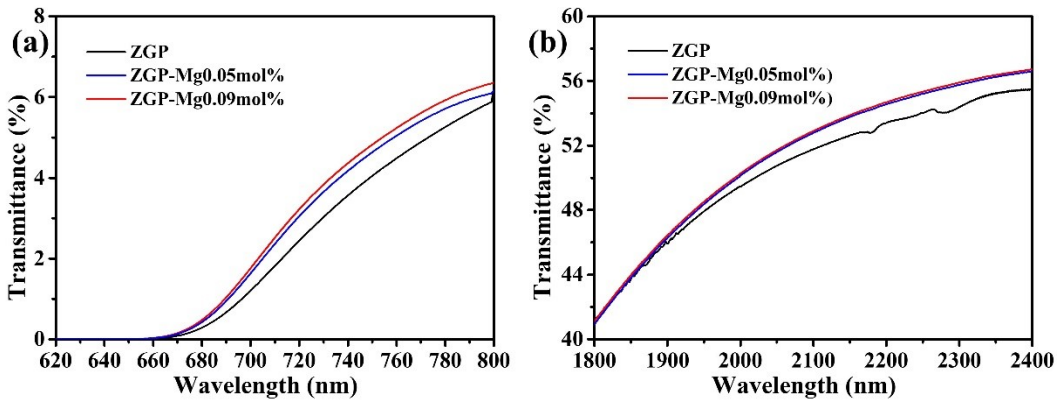

Figure S8. Amplified transmission spectra of ZGP and magnesium-doped ZGP at cut-off edge region (a) and near-infrared region (b).

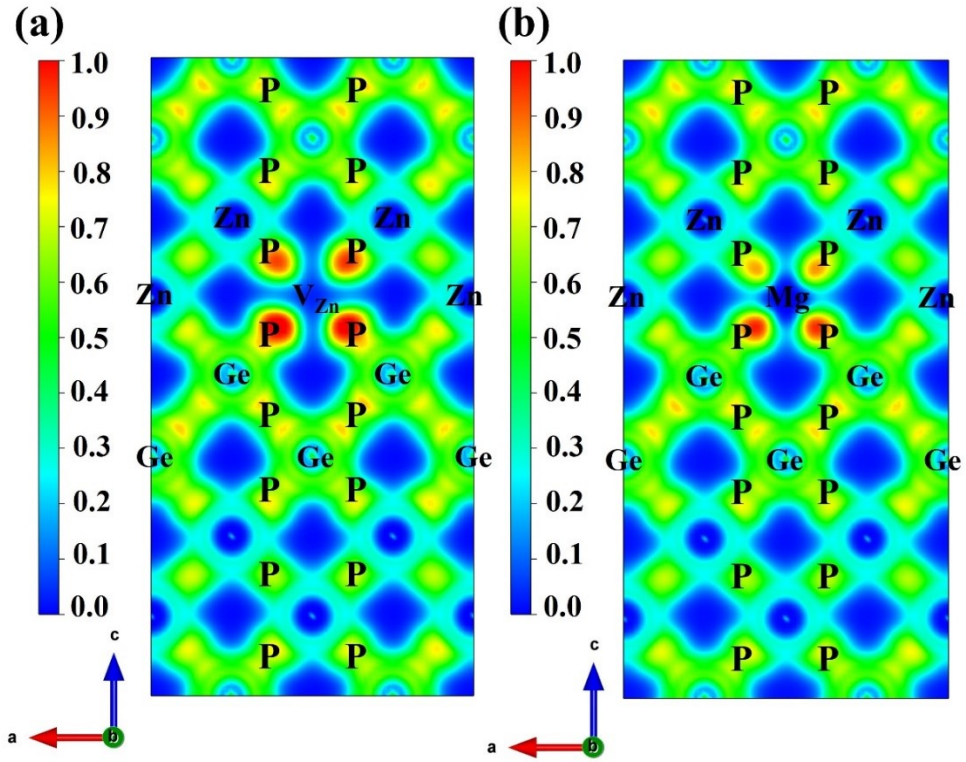

Figure S9. Electron localization function maps of (a) ZGP-V_{Zn} structure, and (b) ZGP-Mg structure.

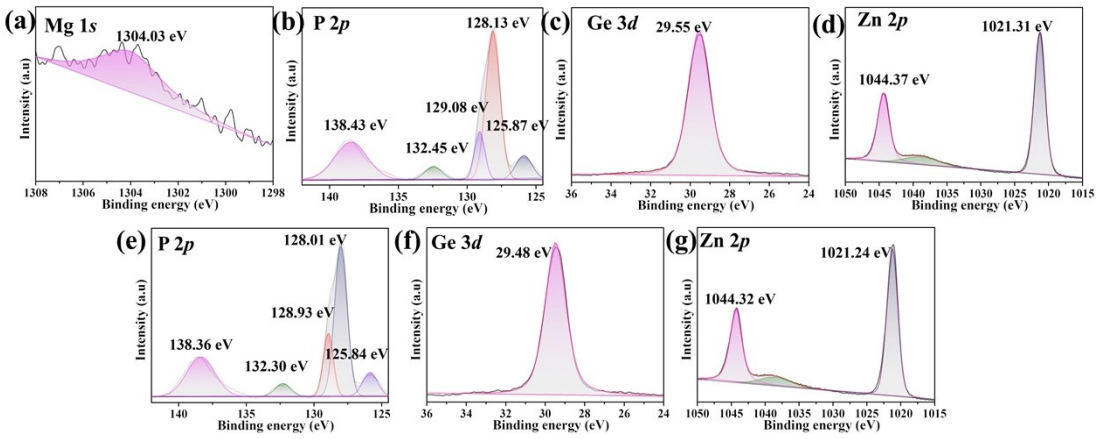

Figure S10. The high-resolution XPS spectra of (a) Mg 1*s*, (b) Zn 2*p*, (c) Ge 3*d* and (d) P 2*p* orbitals in ZGP-M2 crystal; (e) Zn 2*p*, (f) Ge 3*d* and (g) P 2*p* orbitals in ZGP crystal.

References

1. J. P. Perdew, K. Burke and M. Ernzerhof, Generalized gradient approximation made simple, *Phys. Rev. Lett.*, 1996, **77**, 3865-3868.
2. S. Maintz, V. L. Deringer, A. L. Tchougreeff and R. Dronskowski, Analytic projection from plane-wave and PAW wavefunctions and application to chemical-bonding analysis in solids, *J. Comput. Chem.*, 2013, **34**, 2557-2567.
3. S. Maintz, V. L. Deringer, A. L. Tchougreeff and R. Dronskowski, LOBSTER: a tool to extract chemical bonding from plane-wave based DFT, *J. Comput. Chem.*, 2016, **37**, 1030-1035.
4. R. Dronskowski and P. E. Bloechl, Crystal orbital Hamilton populations (COHP): energy-resolved visualization of chemical bonding in solids based on density-functional calculations, *J. Phys. Chem.*, 1993, **97**, 8617-8624.
5. V. L. Deringer, A. L. Tchougréeff and R. Dronskowski, Crystal orbital hamilton population (COHP) analysis as projected from plane-wave basis sets, *J. Phys. Chem. A*, 2011, **115**, 5461-5466.
6. S. Lany and A. Zunger, Assessment of correction methods for the band-gap problem and for finite-size effects in supercell defect calculations: Case studies for ZnO and GaAs, *Phys. Rev. B*, 2008, **78**.
7. Y. Koyama, H. Arai, I. Tanaka, Y. Uchimoto and Z. Ogumi, First principles study of dopant solubility and defect chemistry in $LiCoO_2$, *J. Mater. Chem. A*, 2014, **2**, 11235-11245.
8. Q. Fan, S. Zhu, B. Zhao, B. Chen, Z. He, J. Cheng and T. Xu, Influence of annealing on optical and electrical properties of $ZnGeP_2$ single crystals, *J. Cryst. Growth.*, 2011, **318**, 725-728.
9. Y. J. Yang, Y. J. Zhang, Q. T. Gu, H. J. Zhang and X. T. Tao, Growth and annealing characterization of $ZnGeP_2$ crystal, *J. Cryst. Growth.*, 2011, **318**, 721-724.
10. G. D. Zhang, X. T. Tao, S. P. Wang, G. D. Liu, Q. Shi and M. H. Jiang, Growth and thermal annealing effect on infrared transmittance of $ZnGeP_2$ single crystal, *J. Cryst. Growth.*, 2011, **318**, 717-720.

11. X. Zhao, S. F. Zhu and Y. Q. Sun, Growth of $ZnGeP_2$ Single Crystal by Three-Temperature-Zone Furnace, *Advanced Materials Research*, 2011, **179-180**, 945-948.
12. Z. Y. Wang, M. S. Mao, H. X. Wu, Y. B. Ni, C. B. Huang and X. D. Cheng, Study on annealing of infrared nonlinear optical crystal $ZnGeP_2$, *J. Cryst. Growth.*, 2012, **359**, 11-14.
13. H. X. Wu, Z. Y. Wang, Y. B. Ni, M. S. Mao, C. B. Huang and X. D. Cheng, Vertical gradient freeze growth of $ZnGeP_2$ crystals for nonlinear optical applications, *J. Cryst. Growth.*, 2012, **353**, 158-161.
14. G. D. Zhang, X. T. Tao, S. P. Wang, Q. Shi, H. P. Ruan and L. L. Chen, Growth improvement and quality evaluation of $ZnGeP_2$ single crystals using vertical Bridgman method, *J. Cryst. Growth.*, 2012, **352**, 67-71.
15. L. Q. Cao, B. J. Zhao, S. F. Zhu, B. J. Chen, Z. Y. He, D. H. Yang, H. Liu and H. Xie, Annealing and optical homogeneity of large $ZnGeP_2$ single crystal, *Rare Metals*, 2016, **41**, 3214-3219.
16. D. H. Yang, B. J. Zhao, B. J. Chen, S. F. Zhu, Z. Y. He, Z. R. Zhao and M. D. Liu, Growth of $ZnGeP_2$ single crystals by modified vertical Bridgman method for nonlinear optical devices, *Mater. Sci. Semicond. Process.*, 2017, **67**, 147-151.
17. P. G. Schunemann, K. L. Schepler and P. A. Budni, Nonlinear Frequency Conversion Performance of $AgGaSe_2$, $ZnGeP_2$, and $CdGeAs_2$, *MRS Bull.*, 2013, **23**, 45-49.
18. Z. Lv, Y. Shen, Y. Wen, E.-P. Wang, Z.-M. Wang, W.-L. Li, Y. Bo and Q.-J. Peng, High power widely tunable mid-IR (5–7.2 μm) $ZnGeP_2$ optical parametric oscillator pumped by a 2.09 μm laser, *Infrared Phys. Technol.*, 2023, **134**, 104879.